Site specific probability of passive acoustic detection of humpback whale calls from single fixed hydrophones

Tyler A. Helble,[a] Gerald L. D'Spain, John A. Hildebrand, and Gregory S. Campbell
Scripps Institution of Oceanography, University of California at San Diego, La Jolla, California 92093-0701

Richard L. Campbell and Kevin D. Heaney
Ocean Acoustical Services and Instrumentation Systems, Inc., Fairfax Station, Virginia 22039-1409

(Received 9 July 2012; revised 28 February 2013; accepted 20 May 2013)

Passive acoustic monitoring of marine mammal calls is an increasingly important method for assessing population numbers, distribution, and behavior. A common mistake in the analysis of marine mammal acoustic data is formulating conclusions about these animals without first understanding how environmental properties such as bathymetry, sediment properties, water column sound speed, and ocean acoustic noise influence the detection and character of vocalizations in the acoustic data. The approach in this paper is to use Monte Carlo simulations with a full wave field acoustic propagation model to characterize the site specific probability of detection of six types of humpback whale calls at three passive acoustic monitoring locations off the California coast. Results show that the probability of detection can vary by factors greater than ten when comparing detections across locations, or comparing detections at the same location over time, due to environmental effects. Effects of uncertainties in the inputs to the propagation model are also quantified, and the model accuracy is assessed by comparing calling statistics amassed from 24 690 humpback units recorded in the month of October 2008. Under certain conditions, the probability of detection can be estimated with uncertainties sufficiently small to allow for accurate density estimates. © *2013 Acoustical Society of America*. [http://dx.doi.org/10.1121/1.4816581]

PACS number(s): 43.30.Sf, 43.60.Uv, 43.80.Ka, 43.60.Cg [MCH] Pages: 2556–2570

I. INTRODUCTION

A common mistake in passive acoustic monitoring of marine mammal vocalizations and other biological sounds is to assume many of the features in the recorded data are associated with properties of the marine animals themselves, without accounting for other important aspects. Once a sound is emitted by a marine animal, its propagation through the ocean environment can cause significant distortion and loss in energy.[1] These environmental effects can be readily seen in the ocean-bottom-mounted acoustic data recorded in California waters that are presented in this paper. Spatial variability in bathymetry at shallow-to-mid-depth monitoring sites can be significant over propagation distances typical of those for low (10 to 500 Hz) and mid (500 to 20 kHz) frequency calling animals. Bathymetric effects can break the azimuthal symmetry so that the detection range becomes a function of bearing from the data recording package. In addition to this spatial variability, the site-specific propagation characteristics change over time due to changes in water column properties, leading to changes in the sound speed profile.[1] Solar heating during summertime increases both the sound speed and the vertical gradient in sound speed in the shallow waters where many marine mammal species vocalize. Larger near-surface gradients in sound speed refract the sound more strongly toward the ocean bottom. In contrast, surface ducts that often form and deepen during wintertime can trap sound near the surface.[2] Depending on the location and depth of the receivers, these changes in sound speed profiles can increase or decrease the detectability of calls.

Detection is a function not only of the properties of the received signal, but also of the noise. Differences in the overall level of the noise (defined in this paper as all recorded sounds excluding calls from marine mammal species) can vary by more than 2 orders of magnitude in energy (i.e., by more than 20 dB). In addition, the spectral character of the noise at each site can differ. For example, the variability as a function of frequency in the noise levels is significantly greater at sites with nearby shipping due to the frequency variability of radiated noise from commercial ships.[3] For a given average noise level, signal detection is more difficult in noise with frequency-varying levels than in noise that is flat (i.e., white noise).

All of these site-specific and time-varying environmental effects must be taken into account when evaluating the passive acoustic monitoring capabilities of a recording system deployed in a given location over a given period of time. They also should be taken into account when comparing the passive acoustic monitoring results collected at one location to those from another location. Therefore, it is important to estimate the site specific probability of detection (P is the true underlying detection, and $\hat{P}$ is its estimate) for species-specific acoustic cues within a dataset. As part of this calculation, it is necessary to estimate the azimuth-dependent range over which the detections can occur for each deployed sensor. These estimates must be frequently updated as environmental properties change. One application

[a]Author to whom correspondence should be addressed. Electronic mail: thelble@ucsd.edu

where these site-specific and time-varying environmental effects are particularly important to take into account is in estimating the areal density of various marine mammal species using passive acoustic data.

Significant progress has been made recently in estimating marine mammal population densities using passive acoustic monitoring techniques, most notably in the Density Estimation for Cetaceans from passive Acoustic Fixed sensors (DECAF) project.[4] In addition to being of basic scientific interest, information on population densities is important in regions of human activities, or potential activities, to properly evaluate the potential impact of these activities on the environment. In the DECAF project and in other efforts, a variety of methods are used to calculate $\hat{P}$. It is often derived from estimating the detection function—the probability of detecting an acoustic cue as a function of distance from the receiving sensor.[5] Using distance sampling methods, it is necessary to calculate distances to the vocalizing marine mammal, often a time-consuming task in which multiple sensors for localization are usually needed. Additionally, the detection function may need to be recalculated as environmental parameters change, particularly for low- and mid-frequency vocalizations.

When single fixed sensors are used for density estimation, the probability of detection must be estimated in part from acoustic propagation models. For marine mammals vocalizing at high frequencies (greater than 20 kHz), simple spherical spreading plus frequency dependent absorption models may be sufficient. Küsel *et al*.[6] and Benda-Beckman *et al*.[43] demonstrated the use of spherical spreading plus absorption models in estimating the density of Blainville's beaked whales (*Mesoplodon densirostris*) from passive acoustic recordings. For whales vocalizing at lower frequencies, full wave field acoustic models are necessary, and the uncertainties in the input parameters in these models can lead to large uncertainties in $\hat{P}$.

A growing number of single fixed acoustic sensor packages have been located in the southern California Bight since 2001. Each High-frequency Acoustic Recording Package (HARP),[7] contains a hydrophone tethered above a seafloor-mounted instrument frame, and is deployed in water depths ranging from 200 m up to about 1000 m. Analysts monitor records from these packages for a variety of marine mammal species, including humpback whales (*M*egaptera novaeangliae). Humpback songs consist of a sequence of discrete sound elements, called units, that are separated by silence.[8] Traditionally, analysts mark the presence of humpback whales within a region by indicating each hour in which a vocalization occurred. The recent development of a generalized power-law (GPL) detector for humpback vocalizations[9] has provided the ability to count nearly all human-detectable humpback units within the acoustic record. However, comparing statistics from calling activity between HARP sensors, between seasons, and across years is still constrained by the ability to estimate the spatial and temporal-varying P for these vocalizations, and the areal coverage in which these vocalizations are detected. Comparing activity between geographical locations or at the same location over time without accounting for the acoustic propagation properties of the environment can be extremely misleading, as the probability of detection can vary by factors of 10 or more as shown in Sec. III C.

This paper focuses on three geographical areas off the coast of California, each with distinct bathymetry, ocean bottom sediment structure, sound speed profiles, and ocean noise conditions. This study highlights the variability that bathymetric and other environmental properties create when calculating $\hat{P}$ for humpback whales. Section II gives a brief description of humpback whale activity in the north Pacific, followed by a description of bathymetric and environmental conditions at the three HARP locations off the California coast. This section also highlights the data collection and analysis effort to date for these three HARP locations. Section III outlines the acoustic modeling used to determine $\hat{P}$ for each of the three HARP locations, with the environmental and bathymetric information described in Sec. II B as inputs to the model. Estimates of P are presented for each of the three sites as well as uncertainties for these estimates. Section IV explores the accuracy of the model by comparing detection statistics of 24 690 humpback units from the data collection effort to statistics generated from the model. Section V discusses the importance of various input parameters to the model, giving insight into ways to minimize uncertainty in $\hat{P}$. Additionally, a discussion on the potential for accurate density estimation at the three locations is given. Section VI summarizes the conclusions from this work.

II. PASSIVE ACOUSTIC RECORDING OF TRANSITING HUMPBACK WHALES OFF THE CALIFORNIA COAST

A. The humpback whale population off California

Humpback whales in the north Pacific Ocean exhibit a dynamic population distribution driven by seasonal migration and maternally directed site fidelity.[10–12] They typically feed during spring, summer, and fall in temperate to near polar waters along the northern rim of the Pacific, extending from southern California in the east northward to the Gulf of Alaska, and then westward to the Kamchatka peninsula. During winter months, the majority of the population migrates to warm temperate and tropical sites for mating and birthing.

Although the International Whaling Commission only recognizes a single stock of humpback whales in the north Pacific,[13] good evidence now exists for multiple populations.[10–12,14–17] Based on both DNA analysis[12] and sightings of distinctively-marked individuals,[11] four relatively separate migratory populations have been identified: (1) The eastern north Pacific stock which extends from feeding grounds in coastal California, OR, and Washington to breeding grounds along the coast of Mexico and Central America; (2) the Mexico offshore island stock which ranges from as yet undetermined feeding grounds to offshore islands of Mexico; (3) the central north Pacific stock which ranges from feeding grounds off Alaska to breeding grounds around the Hawaiian Islands; and (4) the western north Pacific stock which extends from probable feeding grounds in the Aleutian Islands to breeding areas off Japan.[11,17–20]

Within the northeastern Pacific region, where the data presented in this paper were collected, photo-ID data indicate migratory movements of humpback whales are complex; however, a high degree of structure exists. Long-term individual site fidelity to both breeding and feeding habitats for the two populations that migrate off the U.S. west coast [populations (1) and (2) above] has been described.[11] The mark-recapture population estimate from 2007/2008 for California and Oregon is 2043 and with a coefficient of variation (CV) of 0.10, this estimate has the greatest level of precision.[21] Mark-recapture data also indicate a long-term increase in the eastern north Pacific stock of 7.5% per year,[21] although short-term declines have occurred during this period, perhaps due to changes in whale distribution relative to the areas sampled. Intriguing variations in seasonal calling patterns between the three data recording sites reported on in this paper have been observed,[22] suggesting that the animals' behavior may differ among these three habitats.

Based on the humpback song recorded at many locations off the coast of California, six representative units were selected as inputs to the acoustic propagation model, and are shown in Fig. 1. These commonly recorded units of a humpback song represent diversity in length, frequency content, and number of harmonics—all of which influence the probability of detecting the units. Vocalizations were selected from a different data source than the HARP recordings so as to capture high signal-to-noise ratio (SNR) vocalizations near to the source, minimizing attenuation and multipath effects.[23]

B. HARP recording sites

Three HARP locations were selected for this study. Site SBC (34.2754°, −120.0238°) is located in the center of the Santa Barbara Channel, site SR (36.3127°, −122.3926°) is on Sur Ridge, a bathymetric feature 45 km southwest of Monterey, and site Hoke (32.1036°, −26.9082°) is located on the Hoke seamount, 800 km west of Los Angeles. A map of coastal California showing the HARP locations, the Santa Barbara Channel commercial shipping lanes, and commercial shipping traffic densities is presented in Fig. 2. Acoustic data collected at each of these sites indicates the occurrence of a humpback song over much of the fall, winter, and spring.

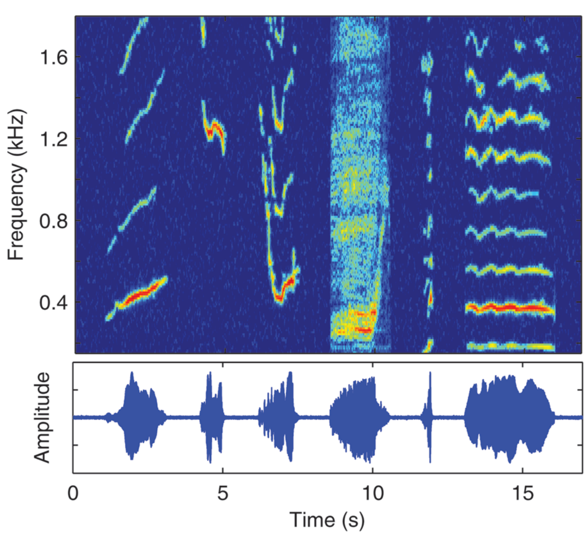

FIG. 1. Six representative humpback whale units used in the modeling. Units labeled 1–6 from left to right.

1. Bathymetry

The bathymetry for each of the three sites can be seen in the upper row of Fig. 3. Bathymetry information for site SR and site SBC was collected from the National Oceanographic and Atmosphere Administration (NOAA) National Geophysical Data Center U.S. Coastal Relief Model.[24] Bathymetry information for site Hoke was collected by combining data from the Monterey Bay Aquarium and Research Institute (MBARI) Atlantis cruise ID AT15L24 with data from the ETOPO1 1 Arc-minute Global Relief Model[25] for depths greater than 2000 m. At site SBC the bathymetry forms a basin with the HARP located near the center of the basin at a depth of 540 m. The walls of the basin slope up to meet the channel islands to the south and the California coastline to the north. The HARP at site SR is located at a depth of 833 m on a narrow steep ridge approximately 15 km long with a width of 3 km trending east–west. To the east the ridge slopes upwards to the continental shelf, and to the west is downward sloping to the deep ocean floor. Site Hoke is located near the shallowest point of the Hoke seamount, at a depth of 770 m. The seamount walls slope downward nearly uniformly in all directions to a depth of 4000 m.

2. Ocean sound speed

Sound speed profiles (SSPs) were calculated from conductivity, temperature, and depth (CTD) casts in the NOAA World Ocean Database[26] that was recorded in near proximity to each of the three sites. Several hundred CTD casts were used in the analysis, covering all seasons and for years ranging from 1965–2008. When available, additional CTD casts were taken during the same time period as the HARP deployments.[3] Figure 4 shows a representative sample of the sound speed profiles collected near each of the three sites, with red indicating summer profiles (Jul.–Sept.) and blue indicating winter profiles (Jan.–Mar.). The plots illustrate the effects of warm surface waters in the summer on the sound speed profiles, especially at site SBC and site Hoke, with a deeper mixed layer occurring at site Hoke. The variation between summer and winter profiles is not as prominent at site SR, which is exposed to cooler mixed waters during the summer months than the other two sites.

Solar heating during summertime increases both the sound speed and the vertical gradient in sound speed in the shallow waters where humpbacks vocalize. Larger near-surface gradients in sound speed refract the sound more strongly toward the ocean bottom, influencing the surface area over which sound propagates directly to the hydrophone. Additionally, surface ducts that often form and deepen during wintertime (most clearly seen in the profiles at site Hoke) can trap sound near the surface, influencing the intensity and spectral characteristics of sound propagating to the bottom-mounted hydrophone.

3. Ocean bottom properties

Ocean bottom characteristics are important input parameters to the acoustic propagation model. A combination of methods was used to characterize the bottom at site SBC.

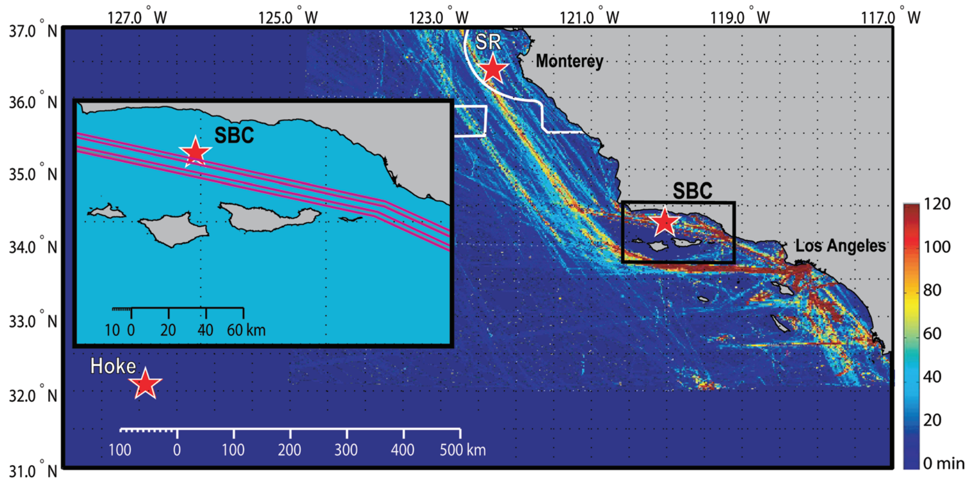

FIG. 2. Map of coastal California showing the three HARP locations: Site SBC, site SR, and site Hoke (stars). The expanded region of the Santa Barbara Channel shows northbound (upper) and southbound (lower) shipping lanes in relation to site SBC. Ship traffic from the Automatic Identification System is shown for region north of 32°N and east of 125°W. The color scale indicates shipping densities, which represent the number of minutes a vessel spent in each grid unit of 1 arc min × 1 arc min size in the month of May 2010. White perimeters represent marine sanctuaries. Shipping densities provided by Chris Miller (Naval Postgraduate School).

Bottom sound speed profile information was obtained from an experiment conducted in the area in which geoacoustic inversion methods were used to calculate the sound speed.[27] The results of this experiment combined with relationships from Hamilton[28,29] suggest that the bottom is comprised of a sediment layer extending beyond 100 m in thickness, containing fine sand material [grain size of $\phi = 2.85$ on the Krumbein phi (ϕ) scale[30,31]]. A separate study was conducted in which sediment core samples were taken very near the location of the HARP. Information from the core suggests a sediment layer extending at least the full length of the 100 m core. The material contained within the core varied from clayey silt to silty clay, with intermediate layers of fine sand.[32] An estimated grain size of $\phi = 7.75$ was used to characterize the core. Most of the transects from the sonar study were nearer to the coastline rather than over the center of the basin, which may partly explain the variability in bottom type between the two studies. It was assumed that these two studies represent the endpoints of uncertainty of the sediment layer in the Santa Barbara channel. Therefore, in addition to these endpoint parameters, a best-estimate value of $\phi = 5.4$ extending to 100 m depth was used for

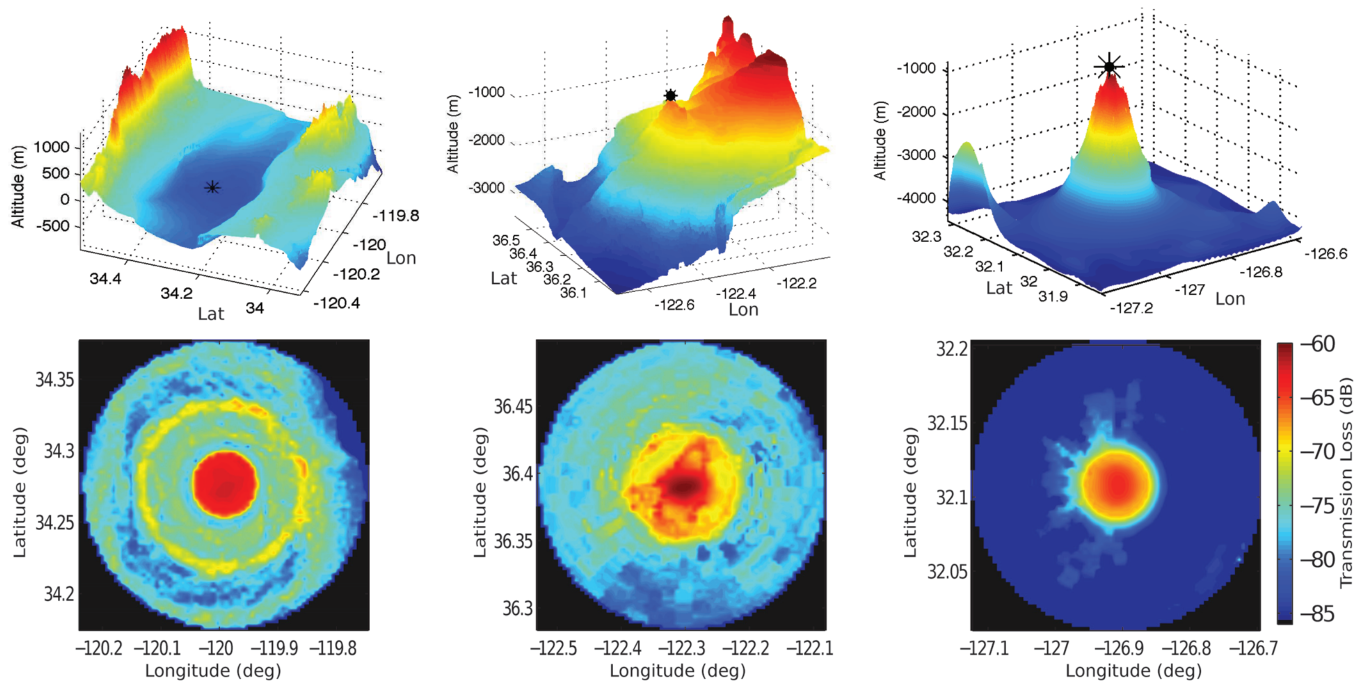

FIG. 3. Bathymetry of site SBC, site SR, and site Hoke (left to right) with accompanying TL plots. The TL plots are incoherently averaged over the 150 to 1800 Hz band and plotted in dB (the color scale for these plots is given on the far right). The location of the HARP in the upper row of plots is marked with a black asterisk.

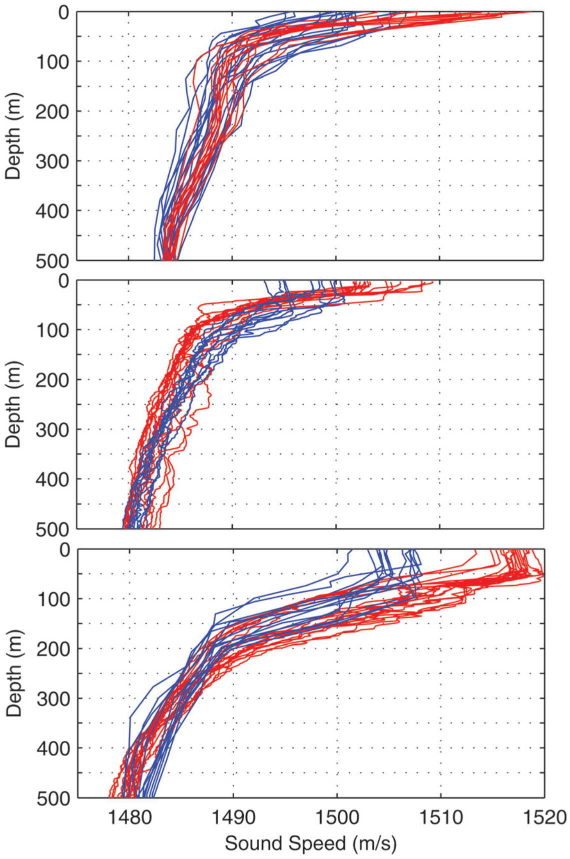

FIG. 4. SSPs for site SBC, site SR, and site Hoke (top to bottom), for winter (blue) and summer (red) months. These data span the years 1965 to 2008.

the modeling effort, corresponding to a silty bottom. Below this layer was assumed to be sedimentary rock (compressional speed = 2374 m/s, density = 1.97 g/cm^3, attenuation = 0.04 dB/m/kHz).

Submersible dives conducted by MBARI along with sediment cores were used to characterize the bottom at site SR. Correspondence with Gary Greene (Moss Landing Marine Laboratories) suggests the ridge itself is thought to be mostly deprived of sediment and composed of sedimentary rock. Surrounding the ridge is sediment covered seafloor—the region east of the ridge contains sediments mostly consisting of fine sand ($\phi = 3$). To the west, the sediment is characterized by clayey silt ($\phi = 7$).[33,34] Eleven sediment cores are available in this region to a depth of only 1 m below the ocean-sediment interface, and so the thickness of the sediment layer is unknown. The best estimate at this site assumes sedimentary rock (compressional speed = 2374 m/s, density = 1.97 g/cm^3, attenuation = 0.04 dB/m/kHz), devoid of sediment out to a range of 4 km from the HARP's location. Beyond the ridge, the sedimentary rock is assumed to have a 10-m sediment cover. Ideally, the modeling would incorporate range and azimuth dependent sediment type—fine sand to the east and clayey silt to the west. However, to increase the speed of the computations, the "best" estimate used in the model assumes the sediment layer is uniform with an average grain size of $\phi = 5$. Since the exact sediment type and layer thickness are unknown, the endpoints for the bottom parameters allow the sediment structure to range from the thickest and most acoustically absorptive (sediment thickness of 50 m and clayey silt, $\phi = 7$), to least absorptive (sediment thickness of 1 m consisting of fine sand, $\phi = 3$).

For site Hoke, sediment samples were collected from the Alvin submarine in 2007 during the deployment of the HARP. Correspondence with David Clague (MBARI) suggests that the rock samples contain common alkalic basalt samples with minimal vesicles. Pictures of the HARP at its resting location on the seamount confirm that the hydrophone is surrounded by this type of rock. No sediments were observed at this site, and sediment deposit is not expected on the slopes of the seamount due to steep bathymetry and strong ocean currents. Detailed studies on the composition of nearby seamounts[35] in combination with Hamilton's[28,29] study suggest that the density of this rock can range from just over 2.0 to 3.0 g/cm^3, with corresponding compressional wave speeds ranging from 3.5 to 6.5 km/s. A best estimate was chosen using a density of 2.58 g/cm^3, compressional speed of 4.5 km/s, and attenuation of 0.03 dB/m/kHz. It was assumed that the uncertainties in the bottom properties on the seamount could span the documented range of values for basalts. This site is the one in which shear propagation likely plays an important role—however, it was not included due to limitations of the acoustic model.

4. Ocean noise levels

The ocean noise was characterized at each site using 75 s samples taken every hour of the HARP recordings over the 2008–2009 calendar year. No data were available from Hoke during June to August, so the noise was characterized using the remaining nine months of data. Figure 5 shows the noise spectrum levels at each of the three sites, with the 90th percentile, 50th percentile, and the 10th percentile noise levels illustrated. The percentile bands were determined from the integrated spectral density levels over the 150 to 1800 Hz band. The gray shaded area in each plot represents the 10th and 90th percentile range from 30 min of HARP recordings used to represent wind-driven conditions over which $\hat{P}$ will be characterized during model simulations.

Noise levels at site SBC can change drastically over short time scales, sometimes varying between extremal values within an hour. The shallow bathymetry shields the basin from sound carried by the deep sound channel, creating at times an extremely low-noise-level environment. However, the channel is also one of the busiest shipping lanes worldwide,[3] and so local shipping noise makes a significant contribution at this site (see Fig. 2). The upper plot in Fig. 5 illustrates the variation in the noise spectrum level with frequency, especially at high noise levels, indicating the presence of a large transiting vessel. Noise at site SR is characterized by wind-driven ocean surface processes, distant shipping, and local shipping. Sur Ridge is exposed to noise from the west traveling in the deep sound channel. Therefore, the lowest noise level times at this site are higher in level than the lowest-level times recorded at site SBC. Although not as prominent as site SBC, large ships do occasionally pass near to site SR, creating more variation across frequency than site Hoke, but less variation across frequency than site SBC. Ocean noise at site Hoke is the least variable

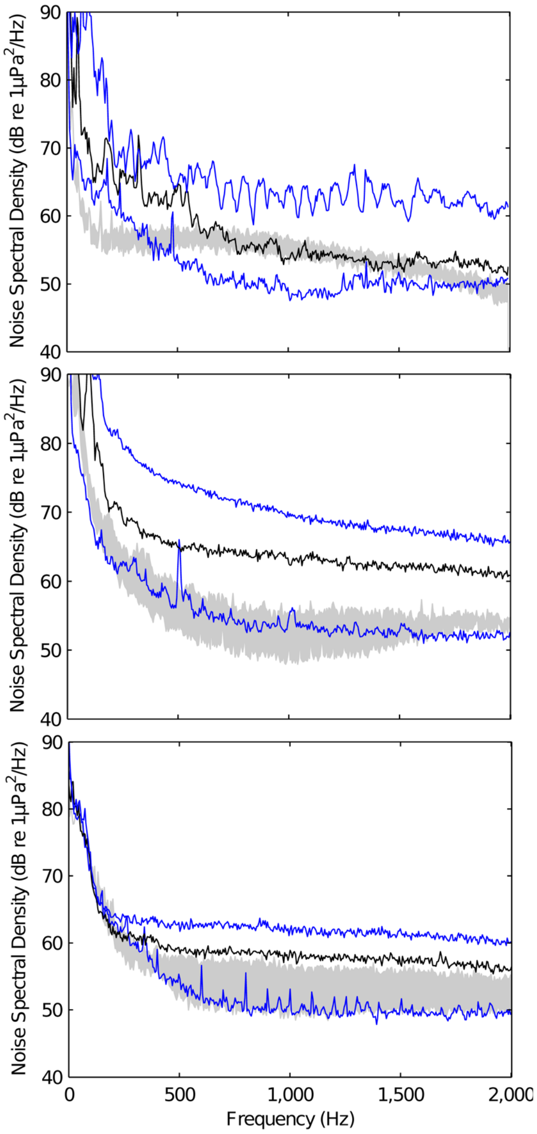

FIG. 5. (Color online) Noise spectral density levels for site SBC, site SR, and site Hoke (top to bottom). The curves indicate the 90th percentile (upper blue), 50th percentile (black), and 10th percentile (lower blue) of frequency-integrated noise levels for 1 year at site SBC and site SR, 9 months at site Hoke. The gray shaded area indicates 10th and 90th percentile levels for wind-driven noise used for modeling.

both spectrally and temporally among the three sites studied. The seamount is exposed to noise from all directions, and the HARP is exposed to noise traveling in the deep sound channel. However, nearby shipping noise is rare for this area of the ocean, and so the noise levels are much less variable than those found at the other two sites. HARP instrument noise can be seen in the lowest percentile curves for all three sites, where hard drive disk read/write events create narrowband contamination.

C. Probability of detection with the recorded data

Acoustic data were recorded at site SBC from April 2008 to January 2010, at site SR from February 2008 to January 2010, and at site Hoke from September 2008 to June 2009. The GPL detector was used to mark the start-time and end-time of nearly every human identifiable unit in the records, resulting in approximately 2 300 000 marked units. The GPL detector is a transient signal detector based on Nutall's power-law processor,[36] which is a near-optimal detector for identifying signals with unknown location, structure, extent, and arbitrary strength. The GPL detector is built on the theory of the power-law processor with modifications necessary to account for drastically changing ocean noise environments, including non-stationary and colored noise generated from shipping. The GPL detector has an average false alarm rate of approximately 5% at the detector threshold used in this research and for the datasets at hand. Therefore, trained human analysts eliminated the false detections manually, using a graphical user interface (GUI), which is part of the GPL software. The GUI allows the analysts to accept or reject large batches of detections at a time, allowing for a much quicker data analysis time when compared to reviewing each detection individually. This pruning effort required approximately 2 weeks (112 h) of trained human analyst time for the total 54 months of recorded data. Statistics obtained from the data analysis effort were used to verify the accuracy of the probability of detection modeling effort, discussed in Sec. III.

III. PROBABILITY OF DETECTION—MODELING

The accuracy of estimating P relies on characterizing the range, azimuth, and depth dependent detection function in accordance with the detector used. In this paper, the variation in depth of calling animals is not fully accounted for in the modeling, so that the detection function, $g(r,\theta)$, is taken as a function of range, r, and azimuth, θ, only. The detection function measures the probability of detection from the hydrophone out to the maximum radial distance (w) in which detection is still possible, over all azimuths. The azimuthal dependence is added to the standard equation to emphasize the complexity caused by bathymetry. The probability of detection within a given area is then calculated by

$$\hat{P} = \int_0^w \int_0^{2\pi} g(r,\theta)\rho(r,\theta) r dr d\theta, \quad (1)$$

where $\rho(r,\theta)$ represents the probability density function (PDF) of whale calling locations in the horizontal plane.[5] Throughout this study, a homogeneous random distribution of animals over the whole area of detection, πw^2, is assumed, and so $\rho(r,\theta) = (1/\pi w^2)$. One way of calculating the detection function is to use a localization method to tabulate distances to whale vocalizations within an acoustic record. An appropriate parametric model for $g(r,\theta)$ is assumed, and $g(r,\theta)$ is estimated based on a PDF of detected distances.[37] This method is often preferred because variables that influence the detection function, such as source level (SL) and acoustic propagation properties, can remain unknown. From the single hydrophone data used in this analysis, tabulating distances to vocalizing animals using localization methods is not possible. Instead, a two-dimensional (2D) acoustic propagation model is used to estimate P within a geographic area. This method requires knowledge about the acoustic environment and the source, and in general is more demanding and perhaps less accurate than methods in which distances to animals can be estimated. However, this method does have some advantages over distance estimation methods. Mainly, a parametric model is not assumed for $g(r, \theta)$, meaning the detection function can both increase and decrease with range. This variation in range is often overlooked using distance methods because high localization accuracy is necessary, and many distances need to be calculated to make these variations statistically significant. Additionally, the use of single fixed sensors for acoustic monitoring can reduce the complexity and cost of the monitoring data acquisition system when compared to localizing systems.

Recent research results have been published on the successful characterization of $\hat{P}$ for detecting marine mammals from single fixed omni-directional sensors, some of which use acoustic models for calculating the detection function.[6,37,38] Most of these studies have involved higher frequency odontocete calls, such as those from beaked whales (family *Ziphiidae*), although some studies have included baleen whales. For higher frequency calls typical of odontocetes, the high absorption of sound with range limit uncertainties associated with environmental parameters, and transmission loss (TL) is usually confined to spherical spreading plus absorption. Therefore, the variables that influence $\hat{P}$ the most tend to be associated with the source, such as whale SL, grouping, location, depth, and orientation due to the directionality of high frequency calls. These types of variations often can be modeled as independent random variables with an assumed distribution, characterized by Monte Carlo simulation. Apart from source level, these variables play a minimal role for acoustic censusing of humpback whales. Au *et al.* show that humpback whales tend to produce omni-directional sound over a very limited range in depth.[39] However, due to the lower frequency nature of the humpback vocalizations, variations in sound propagation due to environmental properties become large. Uncertainties in these variations, such as bottom type, sediment depth, water column sound speed, and bathymetry can lead to uncertainties in $\hat{P}$ that overwhelm uncertainties attributed to other processes. To complicate the issue, the pressure field received at the hydrophone depends on these environmental parameters non-linearly.

To understand the influence of individual variables on $\hat{P}$, these variables are grouped into environmental variables and source variables, and an analysis is conducted on each group separately. The main focus is to characterize the influence of the environment. To do so, the source variable properties remain unchanged, assuming a random homogeneous, horizontal distribution of animals, a fixed source depth of 20 m, and a fixed omnidirectional SL of 160 dB rms re 1 μPa @ 1 m for each humpback unit. The dependence of $\hat{P}$ on environmental variables is explored in two stages. In the first stage, variation is limited to a single input parameter, while holding others fixed at best-estimate values. In the second stage, combinations of variables that lead to extremal values of $\hat{P}$ are characterized. After characterizing the influence of environmental variables, a limited analysis of uncertainties associated with variation originating from the source properties is carried out by holding environmental variables fixed at best-estimate values.

A. Approach—numerical modeling for environmental effects

This section describes the method for estimating the probability of detecting humpback units using a single fixed omni-directional sensor. This method is in many ways similar to that described by Küsel *et al.*[6] for Blainville's beaked whales, but with important differences needed to account for the propagation properties of lower frequency vocalizations. To accommodate the complex transmission of lower frequency calls, a full wave field acoustic propagation model is used. Additionally, unlike beaked whale clicks which have distinct and mostly uniform characteristics, humpback units cover a wide range of frequencies and time scales. As such, the probability of detecting individual units varies significantly—this variation comes about both from bias in the GPL detector, as well as the frequency dependent propagation characteristics of the acoustic environment. Since one important application of estimating $\hat{P}$ is density estimation, establishing an average vocalization rate, or cue rate is required. Because a humpback song can be highly variable, selecting a particular type of unit or even a subset of units to use as acoustic cues would lead to inaccurate density estimates as the song changes. Additionally, a classification system would be needed to single out these units from an acoustic record. Counting all units over a wide frequency range overcomes some of the challenges associated with the variation in the humpback song, but adds additional challenges to characterizing $\hat{P}$ for all unit types.

The humpback units shown in Fig. 1 were used to simulate calls originating at various locations within a 20-km radius centered on the hydrophone. For this purpose, the Range-dependent Acoustic Model (RAM)[40] was used to simulate the call propagation from source to receiver, in amplitude and phase as a function of frequency. In previous studies,[6] the passive sonar equation[41] was used to estimate the acoustic pressure squared level at the receiver. However, this method does not account for phase distortion of the signal, necessary for including propagation effects such as frequency-dependent dispersion. In addition, modeling both the acoustic field amplitude and phase as a function of frequency, which then can be inverse-fast Fourier transformed and added to a realization of noise taken from the measured data, allows the synthesized calls to be processed in an identical way to that of the recorded data.

The RAM model is used to calculate the complex pressure field at 0.2 Hz spacing from 150 to 1800 Hz. An inverse fast Fourier transform of this complex pressure field results in a simulated time series with duration 5 s for data sampled at 10 kHz. This window encompasses the longest-duration humpback unit used in this study, with multipath distortion. The convolution of this pressure time series with the original unit yields the simulated unit as received by the sensor. A sample result is shown in Fig. 6. Once the waveform of a unit transmitted from a particular point on the grid is computed, a randomly-chosen HARP-specific noise sample

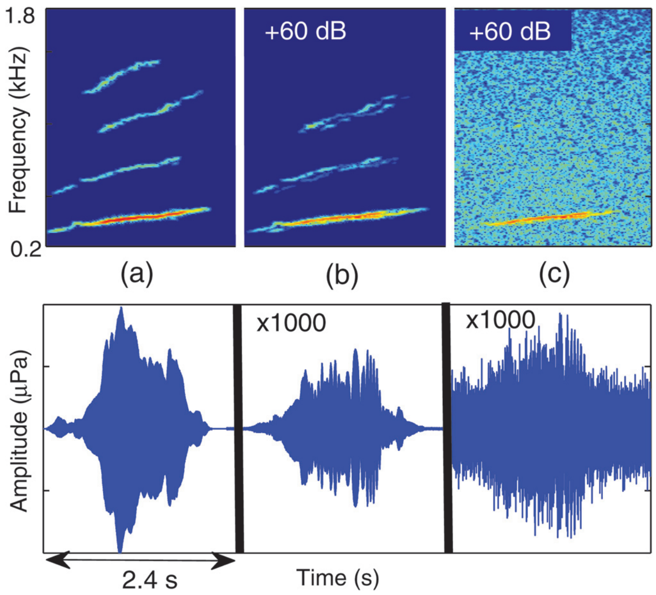

FIG. 6. (a) Measured humpback whale source signal rescaled to a SL of 160 dB re 1 μPa @ 1 m, (b) simulated received signal from a 20 m deep source to a 540 m deep receiver at 5 km range in the Santa Barbara Channel, with no background noise added, (c) simulated received signal as in (b) but with low-level background noise measured at site SBC added. The upper row of figures are spectrograms over the 0.20 to 1.8 kHz band and with 2.4 s duration, and the lower row are the corresponding time series over the same time period as the spectrograms. The received signal and signal-plus-noise time series amplitudes in the second and third columns have been multiplied by a factor of 1000 (equal to adding 60 dB to the corresponding spectrograms) so that these received signals are on the same amplitude scale as the source signal in the first column. This example results in a detection with recorded $\mathrm{SNR_{est}} = 2.54$ dB.

(discussed in Sec. II B) is added and the resulting waveform is passed to the GPL detector. The output of the GPL detector determines whether this unit is detected, and updates the probability of detection for that location on the grid. Calls are simulated over each location on the geographic grid with 20 arc sec spacing. Based on these results, the truncation distance (w) can be chosen, allowing for the calculation of $\hat{P}$ for the area defined by πw^2. This process is repeated with a range of noise samples to produce a curve that links $\hat{P}$ to the monitored noise level as shown in Fig. 7, and discussed further in Sec. III. As previously outlined, these Monte Carlo simulations are also repeated, allowing environmental and source inputs to vary so as to characterize uncertainty in $\hat{P}$.

For purposes of cetacean density estimation, it is sometimes necessary to further restrict the process of detection with an added received SNR constraint. The purpose of this constraint is threefold: (a) To truncate detections to distances that result in stable determination of $\hat{P}$, (b) minimize bias in the detector for varying unit types as outlined in Table II in Helble *et al.*,[9] and (c) limit detections to SNRs easily detectable by human analysts used to verify the output of the detector. Additionally, comparing the estimated SNR in both the simulations and the real datasets allows the accuracy of the model to be assessed. The SNR is defined as

$$\mathrm{SNR} = 10\log_{10}\frac{\langle p_s^2\rangle}{\langle p_n^2\rangle}, \tag{2}$$

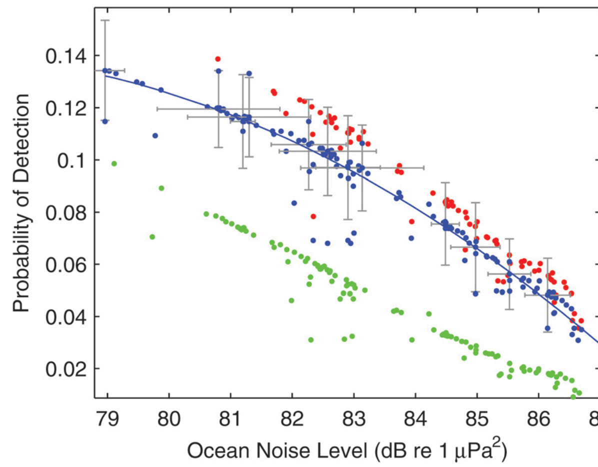

FIG. 7. Site SBC (upper) and site SR (lower) $\hat{P}$ versus noise level for the sediment property and SSP pairing that maximizes $\hat{P}$ (red), the sediment/SSP pairing that minimizes $\hat{P}$ (green), and the best-estimate environmental parameters (blue). Vertical error bars indicate the standard deviation among call unit types, and horizontal error bars indicate the standard deviation of the noise measurement. The noise was estimated by integrating the spectral density over the 150 to 1800 Hz frequency bands using 12 samples of noise within a 75 s period.

where

$$\langle p_{s,n}^2\rangle \equiv \frac{1}{T}\int_0^T p_{s,n}^2(t)dt,$$

and where p represents the recorded pressure of the time series, bandpass filtered between 150 and 1800 Hz, and T is the duration of the time series under consideration.

The GPL detection software automatically estimates the SNR of each detected unit in the recorded data. With real data, the SNR defined in Eq. (2) must be estimated because the recorded pressure of the signal and noise can never be separated completely. This automated estimate of SNR, $\mathrm{SNR_{est}}$, is assisted by the GPL detector, which is designed to identify narrowband features in the presence of broadband noise. Individual frequencies in the spectrogram are identified that correspond to the narrowband humpback signal. These frequency bins also contain noise, and the energy contributed by noise is estimated, by measuring the energy levels in the corresponding bands over a 1-s time period before and after the occurrence of the unit, and then subtracted. The resulting estimates of energy from the signal frequencies are averaged over the duration of the detected unit, and compared to energy in the spectrogram adjacent to the unit within the 150 to 1800 Hz band, resulting in $\mathrm{SNR_{est}}$. Although the exact SNR of simulated data as defined in Eq. (2) could be calculated, SNR is estimated in the same way for both real and simulated data, so that calculations of $\hat{P}$ from simulated data that use an SNR constraint will apply for the analysis of real data.

Choosing an $\mathrm{SNR_{est}} = -1$ dB cutoff helps to minimize the bias in the detector over unit type in addition to limiting incoming detections to levels easily verifiable by human operators. The criteria for selecting detections corresponding to those propagation distances that result in a stable determination of $\hat{P}$ are site specific. For simplicity the same threshold value of -1 dB $\mathrm{SNR_{est}}$ is employed throughout, although adjusting this value based on a number of factors is appropriate, as discussed in Sec. V.

The modeling method outlined in this section is different than most published acoustic-based methods used to derive $\hat{P}$, in which the transmission loss, noise level, and SNR performance of the detector are characterized separately. Using the method proposed in this paper, these quantities are interlinked owing to the site-specific environmental characteristics. Characterizing the detection process jointly gives a more realistic solution, at the cost of substantially greater computational effort.

B. CRAM

The C-program version of the Range-dependent Acoustic Model (CRAM) was developed as a general-purpose $N \times 2D$, full wave field acoustic propagation model. At its core are the self-starter and range-marching algorithm of the RAM 2D parabolic equation (PE) model, originally developed and implemented in FORTRAN by Collins.[40] The PE model is an approximate solution to the full elliptic wave equation, in which the solution is reduced in computational complexity by assuming the outgoing acoustic energy dominates the backscattered energy. In CRAM, setup of the $N \times 2D$ propagation problem is handled automatically for desired receiver output grids in geographic coordinates. The assumptions inherent in the $N \times 2D$ approximation, versus full three-dimensional (3D) propagation modeling, are that horizontal refraction and out-of-plane bathymetric scattering can be neglected in the environment of interest, so that adjacent radials can be computed independently without coupling. The set of independent radials, and the range-marching within each radial, are selected such that the complex pressure for each source-receiver pair is phase-exact in the along-range direction, and approximated in the much less sensitive cross-range direction by a controllable amount. This preservation of spatial coherence allows for beamforming and other post-processing operations which require high fidelity of the complex pressure output.

The RAM Fortran code was ported to the C programming language and refactored for efficiency on modern processor architectures, which have very different relative costs of computation and memory access than older processors. As much of the 2D PE grid setup as possible is reused over multiple frequencies, allowing for a more rapid computation of broadband and time-domain pressure responses. To leverage the multiprocessor capability of modern computers, the program is parallelized over the N independent radials as well as more limited parallelization over frequency and Padé coefficient index, without causing changes to the output.

Environmental inputs are interpolated from a variety of four-dimensional (3D space plus time) ocean models and bathymetry databases as they are needed in the calculations. The model can use standard geoacoustic profiles that are range as well as depth dependent, but its ability to take a scalar mean grain size (ϕ), available from sediment cores or even from the sediment type read off a navigation chart, and convert this information into geoacoustic profiles using Hamilton's relations[28,29] greatly facilitates the problem setup. Additionally, the model can output a variety of file formats including Keyhole Markup Language format that can be imported directly into popular viewers.

C. Results

The resulting TL from the modeling effort as a function of range and azimuth for each site is shown in the lower row of plots in Fig. 3, using the best-estimate environmental parameters as outlined in Sec. II B. These plots were created by placing a horizontal grid of virtual humpback sources at 20-m water depth covering the area out to a 20-km radius from the HARP. The TL is calculated as a function of frequency from the sources to the receiver (HARP) at ranges from 0 (source directly over the HARP) out to 20 km, at all azimuths. To reduce computation time, the principle of reciprocity is used—a single source is placed at the HARP sensor position and the acoustic field is propagated out to each of the grid points (receivers) at 20 m depth. The plotted TL in dB is the result of incoherently averaging over frequency from 150 to 1800 Hz, covering the humpback whale call frequency band. The HARP latitude/longitude position is located in the center of each plot. As these TL plots illustrate, the propagation characteristics at each site are strikingly different. Whereas the TL is comparatively low only in a small-radius circle about the HARP location at site Hoke (the small red circle in the lower right-most plot in Fig. 3), the sound field at site SBC refocuses at a greater range due to interaction with the bathymetry (the outer yellow circular ring surrounding the red circle in the lower left-most plot). This yellow ring indicates that sources at this range can be detected more easily by the HARP than sources at somewhat shorter range. The bathymetry at each site also breaks the azimuthal symmetry so that the detection range is a function of bearing from the HARP package.

1. Values of $\hat{P}$ in wind-driven noise

The simulated probability of detecting Units 1–6 averaged over unit type and in 30 min of wind-driven noise, randomly selected from the HARP data, for sites SBC, SR, and Hoke are shown in Fig. 8. These results use a sound speed profile taken in the month of October with the remaining environmental variables set to best-estimate values as described in Sec. II B. The plots in the uppermost row show $\hat{P}(r, \theta)$, the plots in the middle row show the detection function $g(r)$, averaged over azimuth, and the plots in the lower row show the area-weighted PDF that results. The values of $\hat{P}$ are computed directly from the plots in the upper row; the remaining rows are provided for comparison with other distance sampling methods. The solid lines in the plots from the middle and lower rows indicate values obtained using the -1 dB SNR threshold applied to the GPL output, while the dashed lines illustrate the results in the absence of the -1 dB SNR threshold. The dashed lines clearly show that a substantial fraction of the low-SNR detections occur at distances greater than 20 km for site SBC. Using the SNR threshold, detections for all three sites are limited to $w = 20$ km, resulting in $\hat{P} = 0.1080$ for site SBC, $\hat{P} = 0.0874$ for site SR, and $\hat{P} = 0.0551$ for site Hoke. (For comparison

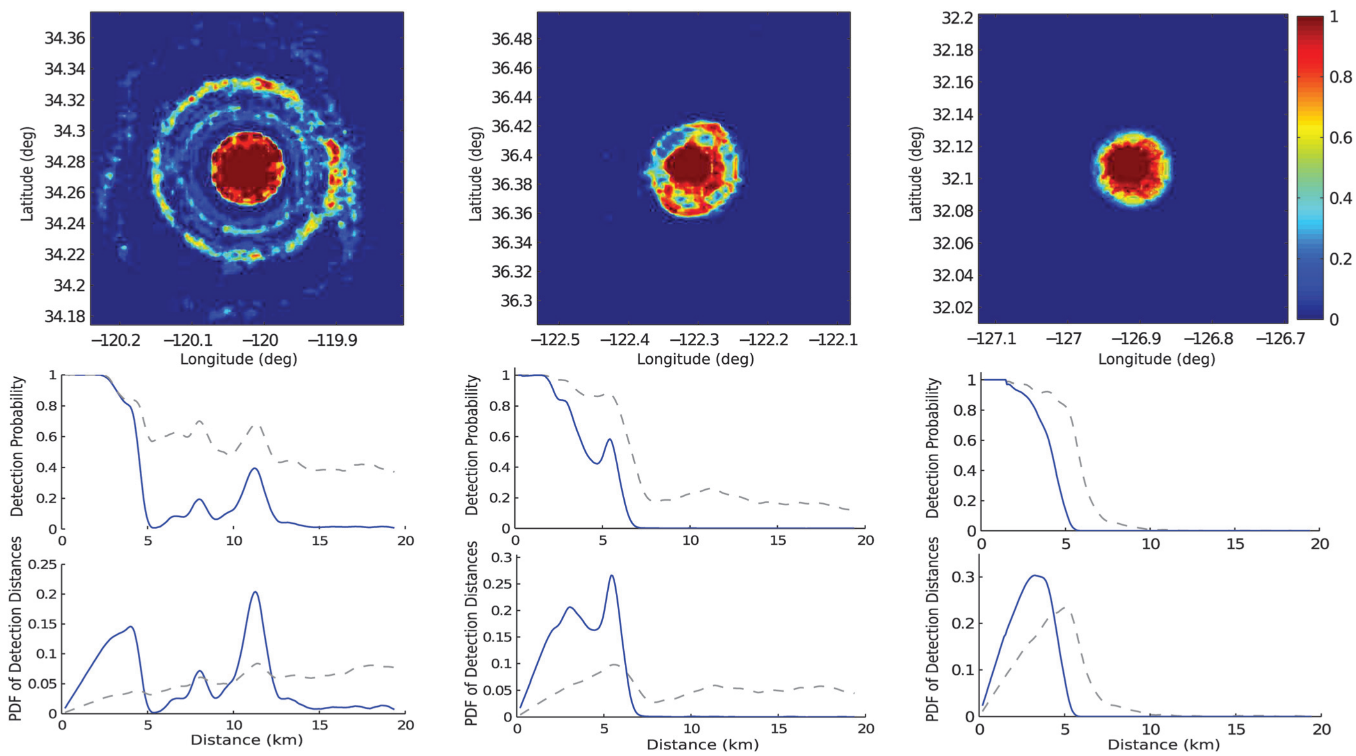

FIG. 8. Probability of detecting a call based on the geographical position of a humpback whale in relation to the hydrophone during periods dominated by wind-driven noise at site SBC (upper left), site SR (upper center), and site Hoke (upper right), averaged over unit type. Assuming a maximum detection distance of $w = 20$ km, average $\hat{P} = 0.1080$ for site SBC, $\hat{P} = 0.0874$ for site SR, and $\hat{P} = 0.0551$ for site Hoke. The latitude and longitude axes in the uppermost row of plots are in decimal degrees. The detection probability functions for the three sites, resulting from averaging over azimuth, are shown in the middle row and the corresponding PDFs of the detected distances are shown in the lower row. Solid (dashed) lines indicate functions with (without) the additional -1 dB SNR_{est} threshold applied at the output of the GPL detector.

purposes, w is set to the same range for all three sites, but in practice w should be calculated as outlined in Sec. III A.) Without the SNR constraint, the probability of detecting humpback units at site SBC can be greater than ten times the probability at site Hoke. The highly structured form of $\hat{P}(r, \theta)$ for both sites SBC and SR, due to the influence of bathymetric features, indicates the necessity of a full 2D simulation of detection. The detailed structure at site SBC also suggests that estimation of the detection function based on localized distances to vocalizing animals as in Marques *et al.*[37] would require an enormous sample size and accurate distance determination, particularly when an SNR threshold is not applied. Note that during a high noise period, such as when a ship is located within the Santa Barbara channel, detections at site SBC are confined to the inner red circular patch (4 km radial distance from HARP). This example emphasizes the necessity of continuous monitoring of noise to calculate $\hat{P}$ as indicated by Fig. 7 and discussed in greater detail in this paper. Figure 9 illustrates an example of the variability in the detection across unit type during a sample of wind-driven noise conditions at site SBC. Units 2 and 5 from Fig. 1 are the ones most difficult to detect owing to high frequency content and brevity, respectively. The decrease in detection of Unit 2 is mainly a consequence of frequency selective attenuation and propagation multipath, and does not result from an intrinsic aspect of the GPL detector. Since the detected sound interacts less with the bottom and travels shorter distances for sites SR and Hoke, the variability in detection across humpback units is less. For site SR, Unit 1 was most detectible with a $\hat{P} = 0.1136$, while Unit 5 was least detectible with a $\hat{P} = 0.0622$. The remaining calls had nearly equal probability of detection (mean $= 0.0872$). Similarly for site Hoke, Unit 1 was most detectible with a $\hat{P} = 0.0651$, while Unit 5 was least detectible with a $\hat{P} = 0.0478$. The remaining calls had nearly equal probability of detection (mean $= 0.0548$).

2. Environmental input variability on $\hat{P}$ in wind-driven noise

The acoustic pressure field calculated by CRAM was recomputed over the full range of environmental input uncertainties at each site to characterize the influence of bathymetry, bottom sediment structure, and SSP on estimates of the probability of detection. Table I illustrates the influence of environmental variables on $\hat{P}$ for the 30-min sample of wind-driven noise at each site. The first row for each site gives extremal examples of the monthly variation in SSP. That is, $\hat{P}$ was recomputed using all SSPs occurring in the month of October (Sec. II B). The values of $\hat{P}$ that led to the largest and smallest values of $\hat{P}$ are shown in Table I, along with a best-estimate value, which was chosen from a typical SSP for the month. All other input variables were fixed at best-estimate values. If the SSP is known within the month of the estimate, the simulation results suggest that changes in the SSP can vary $\hat{P}$ by over 20% for site SBC,

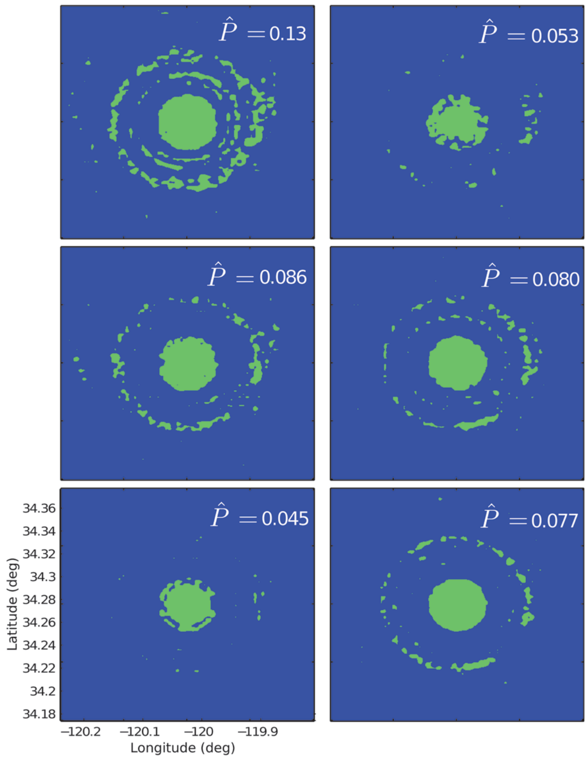

FIG. 9. Geographical locations of detected calls (green dots mark the source locations where detections occur) and associated probability of detection ($\hat{P}$, listed in the upper right corner of each plot) for calls 1–6 (left to right, starting at the top row) in a 20 km radial distance from the hydrophone for a single realization of low wind-driven noise at site SBC. The latitude and longitude scales on each of the six plots are the same as in the upper left-hand plot of Fig. 8.

and over 10% for sites SR and Hoke. The second row of Table I shows the extremal values of $\hat{P}$ if the SSP is chosen over a full year's worth of profiles at each site. For site Hoke and SR, the additional uncertainty is not much larger. However, estimates of $\hat{P}$ at site SBC are more sensitive to the SSP, and the ability to detect humpback units can change between winter and summer by over 300%. The third row in Table I gives extremal and best-estimate values over the full range of uncertainty in the bottom structure (sediment type and thickness) for each of the three sites, as outlined in Sec. II B. Even though site SBC in some ways had the least amount of uncertainty in bottom structure, the difference between the two extremals in sediment type (clayey silt to fine sand), had a large impact on $\hat{P}$, resulting in variations in $\hat{P}$ greater than 300%. The reason for the variability is twofold, the absorption, transmission, and reflection characteristics over these sediment types change significantly over the frequency range of interest, and also because the shallow trough-shaped basin causes the sound field to interact strongly with the bottom. The variation in sediment properties over the range of possible values at site SR was by far the largest source of uncertainty at this location, causing values of $\hat{P}$ to vary by over 100%. In contrast, even though little information was known about the igneous rock at Hoke, the variation over a possible range of values resulted in essentially no differences in estimates of the probability of detection. Owing to the large downward slope of the seamount away from HARP location, the recorded sound interacts very little with the bottom. Additionally, the acoustic impedance mismatch is so high between igneous rock and the water column that the reflection characteristics are very similar over the possible range of igneous rock properties. The last row in Table I for each of the three sites indicates combinations of sediment and SSPs (for the month of October) that led to extremal values of $\hat{P}$. Simulations as well as physical reasoning indicate that SSPs that have summer attributes (strong downward-refracting near-surface conditions) combined with the smallest grain sizes and thickest sediment layers yield the smallest values of detection. Conversely, SSPs that have winter attributes paired with the largest grain size and thinnest sediment layer produce the maximum detection values. Variations over the bottom type at site Hoke combined with monthly variation in SSP did not produce measurable differences with those from holding the bottom type fixed. In summary, the environmental variables that create the most uncertainty in $\hat{P}$ are site specific. Guided by physical intuition, one can use an acoustic model with historical data as input for a given location to identify the main sources of uncertainty, and can quantify that uncertainty, in estimating the probability of detection.

TABLE I. Best-estimate and extremal predictions for $\hat{P}$ for wind-driven noise conditions, given the uncertainty in input parameters of SSP and sediment structure for each site, as outlined in Sec. II B. Each estimate of P assumes the remaining variables are fixed at best-estimate values. The $\hat{P}$ values assume a detection radius of $w = 20$ km from the instrument center.

		Min extremal	Best estimate	Max extremal
SBC	Monthly variation in SSP	0.0823	0.1080	0.1150
	Yearly variation in SSP	0.0823	0.1080	0.2965
	Sediment variation	0.0458	0.1080	0.1887
	Monthly SSP variation + sediment variation	0.0414	0.1080	0.1892
SR	Monthly variation in SSP	0.0778	0.0874	0.0901
	Yearly variation in SSP	0.0778	0.0874	0.0914
	Sediment variation	0.0599	0.0874	0.1010
	Monthly SSP variation + sediment variation	0.0520	0.0874	0.1031
Hoke	Monthly variation in SSP	0.0482	0.0551	0.0565
	Yearly variation in SSP	0.0460	0.0551	0.0565
	Sediment variation	0.0551	0.0551	0.0551
	Monthly SSP variation + sediment variation	0.0482	0.0551	0.0565

An extensive study was not conducted to measure the influence of variation in source properties (i.e., source depth, source level, deviation of horizontal source distribution from homogeneous) on $\hat{P}$. However, simulations using 1000 humpback units were conducted, allowing the SL to vary with a Gaussian distribution (mean = 160 dB re 1 μPa @ 1 m, standard deviation = 2 dB). This amount of variation covers the full range of call levels reported in Au *et al.*,[39] although the true distribution of call levels cannot be determined with the limited data available in this paper. For site SR, allowing the SL to vary holding environmental parameters fixed at best-estimate values resulted in a CV (equal to the ratio of the standard deviation to the mean) of 25.3% about the best-estimate mean of $\hat{P} = 0.0874$. Similarly, allowing the source to vary in depth between 10 and 30 m resulted in even less variation. Both factors, in any combination, result in significantly less variability than that due to the uncertainty of the bottom type at site SR.

3. Influence of ocean noise on $\hat{P}$

Ocean noise has a large influence on $\hat{P}$. The noise in the band of humpback vocalizations can vary appreciably in both level and structure. Since detection is a function of both the noise level (SNR) and the variance of the noise level, a noise model that does not account for long-term changes in noise level or short-term variance in noise level across time and frequency is not sufficient for predicting the performance of the detector, and ultimately $\hat{P}$. Ocean noise was collected from each of the HARP datasets over a wide range of conditions and used as input to the calculation of $\hat{P}$. Figure 7 shows the relationship of $\hat{P}$ versus noise level for sites SBC and SR. The blue dots represent this relationship of $\hat{P}$ versus noise level for best-estimate environmental conditions averaged over all call types, while the green and red dots represent the modeling results using extremal environmental conditions (re Sec. II B), averaged over all call types. The noise was estimated by integrating the spectral density over the 150 to 1800 Hz frequency bands using 12 samples of noise within a 75 s period. An average noise value was then assigned to each 75 s sample of noise used during the simulation. The horizontal error bars represent the standard deviation of the 12 noise measurements. The vertical error bars represent the standard deviation in the probability of detection across unit type. As the noise level decreases, the units can be detected at a farther range, and so can incur greater frequency-dependent attenuation and interaction with the ocean bottom, increasing the variability in detection over unit type. As the noise level increases, the variance of the noise also tends to increase, so that an average of noise level over a 75 s time period becomes less sufficient in characterizing detection performance. A curve composed of two separate exponentials was matched to the blue data points for site SBC. At high noise levels (detail in Fig. 7 inset), the behavior for $\hat{P}$ is dominated by direct path propagation, whereas during low noise conditions, interaction with the bottom and the increase in the area monitored with the square of the increase in detection range tend to dominate the shape of the curve. For site SR, a quadratic polynomial was used to fit the blue dots.

IV. MODEL/DATA COMPARISON

Given the non-overlapping coverage and omnidirectional nature of the HARP sensors, it was not possible to calculate the detection function using source localization methods. Therefore, this approach's results cannot be compared to the results in this paper. For the data processing discussed in Sec. II C, using data recorded in the month of October, an estimate of noise level was made in addition to recording the SNR_{est} of each detected humpback unit. The shaded region in Fig. 10 shows the normalized histogram of recorded humpback units as a function of received SNR_{est} over a 2 dB range of received noise levels. These simulated

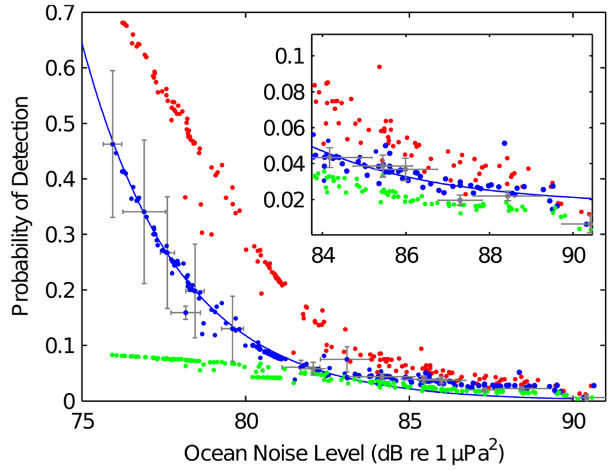

FIG. 10. (Color online) Shaded gray indicates normalized histogram of received SNR estimates (SNR_{est}) for humpback units at site SBC, site SR, and site Hoke (top to bottom). Model best environmental estimates (black line) and model upper environmental estimates (green line). The cyan line indicates best estimate results with 4 km radial calling "exclusion zone" at site Hoke.

results (black and green curves) used SSPs taken during the month of October, and 100 000 simulated calls random homogeneously distributed around the HARP. As with the other simulations, the SL of all units was assumed to be 160 dB re 1 μPa @ 1 m, at a depth of 20 m. Site SBC's normalized histogram of the data processing results was created using 8944 calls over a measured noise range of 78 to 80 dB re 1 μPa, site SR's data histogram was created using 6559 calls over a noise range of 82 to 84 dB re 1 μPa, and site Hoke's data histogram was created using 9187 calls over a noise range of 82 to 84 dB re 1 μPa (all noise values integrated from 150 to 1800 Hz). The simulated histograms were generated using the same 2 dB noise ranges. The SNR and noise levels for each detected unit were estimated using the method described in Sec. III A. The agreement of the simulated and measured histograms for sites SBC and SR suggest that the input best-estimate model parameters and the assumptions about the source properties are quite reasonable. For site SBC, the 5 to 15 dB SNR_{est} range on the horizontal axis of the plot represents calls originating near to the receiver, whose arrival structure is dominated by the direct path. The agreement of the predicted values and measured values in this range suggest that the average unit SL is very close to 160 dB re 1 μPa @ 1 m, which verifies the mean SL estimated by Au *et al*.[39] If the animal locations follow a homogeneous random distribution in this area, the results suggest that the true environmental input parameters are somewhere between best-estimate values and those that maximize $\hat{P}$. Because the simulations considered calls only out to a 20 km distance, the left-hand portion of the histograms do not agree at site SBC. This discrepancy verifies that without a received SNR cutoff and/or higher detection threshold, units are detected at distances greater than 20 km. The shape of each of the histograms at low SNR_{est} (left-hand side of the plots) is shaped by the performance of the GPL detector. The performance of the detector drops sharply as the SNR of received calls drops below −7 dB SNR. As with site SBC, if the calls at site SR are indeed homogeneously distributed, the results suggest that the environmental input parameters set between best-estimate values and those yielding maximum $\hat{P}$ values would best match the measured SNR distribution. In contrast, the observed distribution of received call SNRs at Hoke does not fall within the bounds predicted by the model. This observed distribution can arise from one of two situations: Either the calls are not homogeneously distributed around the HARP, or the calls are homogeneously distributed but detections can occur at much greater distances than the model predicts. It is possible that at this site, the acoustic energy created by shallow sources somehow couples into the deep sound channel to allow for very long range detection by the HARP approximately at the sound channel axis depth. If the calls are originating only within 20 km of the HARP, they must occur at distances greater than 4 km from the HARP. One possibility that would lead to a 4 km "exclusion zone" is that the humpback whales are transiting along a narrow migration corridor with a 4 km closest point of approach. Alternatively, perhaps they are avoiding the shallowest portion of the seamount for some reason. The cyan curve in the lowermost plot of Fig. 10 is the result of running the model with calls homogeneously distributed in the area, but excluded within 4 km of the shallowest portion of the seamount.

V. DISCUSSION

The uncertainties in $\hat{P}$ from single fixed sensors due to unknowns in environmental parameters such as sound speed profile, bottom sediment structure, and ocean noise can be large for animal calls at all frequencies. For the mid to low frequencies typical of vocalizations from mysticete whales, these uncertainties generally outweigh the uncertainties associated with the source, such as whale calling depth and source level. For higher frequency vocalizations typical of odontocete whales, the uncertainties associated with environmental parameters other than ocean noise are minimized because the sound attenuates to undetectable levels before considerable interaction with the bottom occurs. Variability in ocean noise levels is still a significant issue at higher frequencies, but the variance in noise levels and the decibel range also tend to be smaller than at lower frequencies.

Under certain conditions, environmental uncertainties using single fixed sensors may be tolerable, especially when comparing calls at a fixed location over time. In this case, the bias in $\hat{P}$ associated with an unknown sediment structure may be large, but since it remains constant over time, it cancels out. On the other hand, the variation in $\hat{P}$ due to changes in the sound speed profile at some locations can be significant when comparing calling activity over seasons. The large influence of SSP on $\hat{P}$ was demonstrated at site SBC, where the SSP between summer and winter creates a threefold change in $\hat{P}$.

As for comparisons of calling activity at different hydrophone locations, uncertainties in estimates of P using single fixed sensors may be acceptable. For example, if the calls are homogeneously distributed at Hoke, the maximum uncertainty in estimates of $\hat{P}$ associated with environmental variability is around 15%. Therefore, it may be possible to use this modeling technique to determine if there are more vocalizations per km^2 at one location compared to another, if the normalized call counts differ by more than the uncertainty in the probabilities of detection at the two sites.

The drastic variation in $\hat{P}$ over both time at a given site, and across sites, highlights the dangers of comparing intra-site and inter-site calling activity without first accounting for environmental effects on the probability of detection. When an SNR constraint is not used as an additional filter on the GPL detector output, the probability of detecting humpback calls at site SBC can be greater than ten times the probability of detecting calls at site Hoke. Even if two sensors are located in regions with similar bathymetric and bottom conditions, differences in noise levels between two sites (or at the same site over time) of just a few decibels can easily change the probability of detection by a factor of 2.

One application that involves quantifying $\hat{P}$ is the estimation of the areal density of marine mammals from passive acoustic recordings of their calling activity. The animal density estimation equation based on measuring cue counts in a given area is given as[42]

$$\hat{D} = \frac{n_u(1-\hat{c})}{K\pi w^2 \hat{P} T \hat{r}}, \tag{3}$$

where $\hat{D}$ is the density estimate, n_u is the number of detected acoustic cues, $\hat{c}$ is the number of false positive detections, K is the number of sensors (for single omni-directional sensors in a monitoring area, as in this paper, $K = 1$), w is the maximum detection range beyond which one assumes no acoustic cues are detected, $\hat{P}$ is the estimated average probability of detection covered by the area πw^2, T is the time period over which the units are tabulated, and $\hat{r}$ is the estimated cue production rate.

The detector design criteria, including the detector threshold and additional constraints placed on the received SNR, can influence the uncertainties in estimates of $\hat{D}$. From results presented in this paper, the uncertainty from environmental parameters in $\hat{P}$ roughly increases with increasing area monitored. One possible approach for minimizing uncertainty is to raise the received minimum SNR threshold to values that correspond with direct path transmission from source to receiver. However, doing so decreases the cue counts for the time period of interest, thereby increasing the statistical variability of the estimates. Additionally, decreasing the monitored area could cause a violation of the assumption that calls are homogeneously distributed in space. Therefore, accurate density estimation involves an optimization problem of determining how to estimate the various quantities in the equation for animal density such the uncertainty in $\hat{D}$ is minimized.

Running a high fidelity, full wave field, ocean acoustic model using a span of likely environmental variables from historical data as input is an instructive and cost-efficient way of determining the environmental variables that most influence $\hat{P}$ for a particular location. Results from the model help determine where best to allocate resources to decrease the uncertainty in $\hat{P}$. In some cases, *in situ* propagation calibration using a controlled acoustic source may be warranted to correctly characterize the bottom properties. Alternatively, bottom geoacoustic information can be derived from sediment cores and published empirical relations. In other cases, resources may be best allocated to recording monthly changes in the SSP, perhaps even weekly during transitional months in the fall and spring. Oceanographic models, coupled with satellite-based measurements such as sea surface temperature, may provide sufficient information on the temporal variability of the water column. In general, ancillary environmental information may be very helpful in reducing the uncertainty in $\hat{P}$ to acceptable levels.

Site selection for sensor deployment in passive acoustic monitoring also plays a vital role in reducing uncertainties in $\hat{P}$. Results from this paper suggest that hydrophones are best deployed in areas where the bathymetry, bottom type, and sound speed profiles are well characterized. If this information is not available, selecting locations that minimize sound interaction with the bottom will help reduce uncertainties in $\hat{P}$. Shallow bowl-shaped or trough-shaped basins tend to produce the most uncertainty in $\hat{P}$ since sound interacts the most with the bottom, and temporally-varying SSPs will focus this propagating sound in circular regions of temporally-varying distances from the hydrophones. Since the area monitored increases with the square of the distance from the hydrophone, small changes in the ranges of these acoustic convergence zones can have a large effect on the amount of area from which an acoustic signal can be detected.

Results presented from the model/data comparison suggest that low and mid frequency calling whales can be used as acoustic sources of opportunity for geoacoustic inversion of ocean bottom properties. If the whale source level, source depth, and source distribution, and ocean noise and SSP are known, then statistics on the distribution of the received SNR of calls at the receiver can be compared with acoustic models to significantly constrain the effective properties of the bottom. An example of the feasibility of this geoacoustic inversion approach was demonstrated at site SR (middle plot in Fig. 10), where a good match between the recorded data and model suggest that the sediment thickness ranges between 1 and 10 m before encountering sedimentary rock. Running the model with 50 m sediment thickness gives a very poor model/data fit. If information on the SL and distribution of humpbacks in this region could be measured, then the inversion results on sediment thickness could be presented with reasonable confidence.

The uncertainties in $\hat{P}$ presented in this paper assume complete accuracy of the CRAM model. The RAM core of the CRAM model is based on an estimate of a solution to the acoustic wave equation, and therefore is not exact. The model does not incorporate the shear properties of the bottom, which could influence the accuracy of the model, especially with higher density bottom types, such as at site Hoke. The model also does account for acoustic backscatter.

VI. CONCLUSIONS

Acoustic propagation modeling is a useful tool for quantifying the probability of detection and the associated uncertainties in those measurements for single fixed sensors. For low and mid frequency vocalizations, simple propagation models are not sufficient for estimating $\hat{P}$. Rather, a more sophisticated model that includes bathymetry, sound speed, bottom characteristics, and site specific noise to estimate the complex pressure field at the receiver is necessary. The environmental parameters that create the most uncertainty in the probability of detecting a signal are site specific; using an acoustic model with historical environmental data is an effective way for determining where best to allocate resources for minimizing the uncertainties in $\hat{P}$. In some instances, the errors associated with the uncertainties in $\hat{P}$ may be sufficiently small, allowing for reasonable density estimates using single fixed sensors. Results from this study suggest that comparing calling activity at the same sensor over time or across sensors in different geographical locations without first accounting for $\hat{P}$ is a questionable procedure, as the probability of detecting calls can vary by factors of 10 or more for low and mid frequency calling whales.

ACKNOWLEDGMENTS

The authors are extremely grateful to Glenn Ierley, Megan McKenna, Amanda Debich, and Heidi Batchelor, all at Scripps Institution of Oceanography, for their support of this research. Gary Greene at Moss Landing Marine Laboratories and David Clague and Maria Stone at MBARI were instrumental in obtaining bathymetric and ocean bottom information used in this study. Bathymetry data collected from R/V Atlantis, cruise ID AT15L24, were provided courtesy of Curt Collins (Naval Postgraduate School) and processed by Jennifer Paduan (MBARI). Shipping densities were provided by Chris Miller (Naval Postgraduate School). Special thanks to Sean Wiggins and the entire Scripps Whale Acoustics Laboratory for providing thousands of hours of high quality acoustic recordings. The CRAM acoustic propagation code used in this research was written by Richard Campbell and Kevin Heaney of OASIS, Inc., using Mike Collins' RAM program as the starting point. T.A.H. would like to thank the Department of Defense Science, Mathematics, and Research for Transformation Scholarship program, the Space and Naval Warfare (SPAWAR) Systems Command Center Pacific In-House Laboratory Independent Research program, and Rich Arrieta from the SPAWAR Unmanned Maritime Vehicles Lab for continued financial and technical support. Work was also supported by the Office of Naval Research, Code 32, the Chief of Naval Operations N45, and the Naval Postgraduate School.

[1]C. Clay and H. Medwin, *Acoustical Oceanography: Principles and Applications* (Wiley, New York, 1977), Vol. 4, pp. 84–89.

[2]P. Etter, *Underwater Acoustic Modeling and Simulation* (Spon Press, New York, 2003), pp. 82–84.

[3]M. McKenna, D. Ross, S. Wiggins, and J. Hildebrand, "Underwater radiated noise from modern commercial ships," J. Acoust. Soc. Am. **131**, 92–103 (2012).

[4]L. Thomas, T. Marques, D. Borchers, C. Stephenson, D. Moretti, R. Morrissey, N. DiMarzio, J. Ward, D. Mellinger, S. Martin, and P. Tyack, "Density estimation for cetaceans from passive acoustic fixed sensors: Final programmatic report," Technical Report, Center for research into ecological and environmental modeling, University of St. Andrews,

Scotland, UK (2011), http://www.creem.st-and.ac.uk/decaf/outputs/2007-0145-00220Final20Report.pdf/view (Last viewed March 2, 2013).
[5]S. Buckland, D. Anderson, K. Burnham, J. Laake, and L. Thomas, *Introduction to Distance Sampling: Estimating Abundance of Biological Populations* (Oxford University Press, New York, 2001), pp. 1–448.
[6]E. Küsel, D. Mellinger, L. Thomas, T. Marques, D. Moretti, and J. Ward, "Cetacean population density estimation from single fixed sensors using passive acoustics," J. Acoust. Soc. Am. **129**, 3610–3622 (2011).
[7]S. Wiggins, "Autonomous Acoustic Recording Packages (ARPs) for long-term monitoring of whale sounds," Marine Technol. Soc. J. **37**, 13–22 (2003).
[8]R. Payne and S. McVay, "Songs of humpback whales," Science **173**, 585–597 (1971).
[9]T. Helble, G. Ierley, G. D'Spain, M. Roch, and J. Hildebrand, "A generalized power-law detection algorithm for humpback whale vocalizations," J. Acoust. Soc. Am. **131**, 2682–2699 (2012).
[10]C. Baker, L. Medrano-Gonzalez, J. Calambokidis, A. Perry, F. Pichler, H. Rosenbaum, J. Straley, J. Urban-Ramirez, M. Yamaguchi, and O. von Ziegesar, "Population structure of nuclear and mitochondrial DNA variation among humpback whales in the North Pacific," Mol. Ecol. **7**, 695–707 (1998).
[11]J. Calambokidis, E. Falcone, T. Quinn, A. Burdin, P. Clapham, J. Ford, C. Gabriele, R. LeDuc, D. Mattila, L. Rojas-Bracho, J. Straley, B. Taylor, J. Urban, D. Weller, B. Witteveen, M. Yamaguchi, A. Bendlin, D. Camacho, K. Flynn, A. Havron, J. Huggins, and N. Maloney, "SPLASH: Structure of populations, levels of abundance and status of humpback whales in the North Pacific," Technical Report, Cascadia Research Collective, Olympia, WA (2008), http://www.cascadiaresearch.org/SPLASH/SPLASH-contract-Report-May08.pdf (Last viewed March 2, 2013).
[12]C. Baker, D. Steel, J. Calambokidis, J. Barlow, A. Burdin, P. Clapham, E. Falcone, J. Ford, C. Gabriele, U. Gozález-Peral, R. LeDuc, D. Mattila, T. Quinn, L. Rojas-Bracho, J. Straley, B. Taylor, R. Urban, M. Vant, P. Wade, D. Weller, B. Witteveen, K. Wynne, and M. Yamaguchi, "geneSPLASH: An initial, ocean-wide survey of mitochondrial (mt) DNA diversity and population structure among humpback whales in the North Pacific: Final report for contract 2006-0093-008 Principal Investigator: C. Scott Baker," Technical Report, Cascadia Research Collective, Olympia, WA (2008), http://www.cascadiaresearch.org/SPLASH/ NFWF08eneSPLASHinal9Sep08.pdf (Last viewed March 2, 2013).
[13]G. Donovan, "A review of IWC stock boundaries," Reports of the International Whaling Commission (special issue) (1991), pp. 39–68.
[14]J. Johnson and A. Wolman, "The humpback whale, *Megaptera novaeangliae*," Mar. Fish. Rev. **46**, 30–37 (1984).
[15]J. Barlow, "The abundance of cetaceans in California waters. Part I: Ship surveys in summer and fall of 1991," Fish. Bull. **93**, 1–14 (1995).
[16]J. Calambokidis, G. Steiger, K. Rasmussen, J. Urban, K. Balcomb, P. de Guevara, M. Salinas, J. Jacobsen, C. Baker, L. Herman, S. Cerchio, and J. Darling, "Migratory destinations of humpback whales that feed off California, Oregon and Washington," Mar. Ecol.: Prog. Ser. **192**, 295–304 (2000).
[17]J. Calambokidis, G. Steiger, J. Straley, L. Herman, S. Cerchio, D. Salden, U. Jorge, J. Jacobsen, O. von Ziegesar, K. Balcomb, C. Gabriele, M. Dahlheim, S. Uchida, G. Ellis, Y. Miyamura, P. de Guevara, M. Yamaguchi, F. Sato, S. Mizroch, L. Schlender, K. Rasmussen, J. Barlow, and T. Quinn, "Movements and population structure of humpback whales in the North Pacific," Marine Mammal Sci. **17**, 769–794 (2001).
[18]J. Calambokidis, G. Steiger, J. Evenson, K. Flynn, K. Balcomb, D. Claridge, P. Bloedel, J. Straley, C. Baker, O. von Ziegesar, M. Dahlheim, J. Waite, J. Darling, G. Elllis, and G. Green, "Interchange and isolation of humpback whales off California and other North Pacific feeding grounds," Marine Mammal Sci. **12**, 215–226 (1996).
[19]J. Calambokidis, G. Steiger, D. Ellifrit, B. Troutman, and C. Bowlby, "Distribution and abundance of humpback whales (*Megaptera novaeangliae*) and other marine mammals off the northern Washington coast," Fish. Bull. **102**, 563–580 (2004).
[20]R. Urban, C. Alvarez, M. Salinas, J. Jacobsen, K. Balcomb, A. Jaramillo, P. de Guevara, and A. Aguayo, "Population size of humpback whale, *Megaptera novaeangliae*, in waters off the Pacific coast of Mexico," Fish. Bull. **97**, 1017–1024 (1999).
[21]J. Calambokidis, E. Falcone, A. Douglas, L. Schlender, and J. Huggins, "Photographic identification of humpback and blue whales off the US west coast: Results and updated abundance estimates from 2008 field season," Technical Report, Cascadia Research Collective, Olympia, WA (2009), http://www.cascadiaresearch.org/reports/Rep-BmMn-2008-SWFSC-Rev.pdf (Last viewed March 2, 2013).
[22]G. Campbell, T. Helble, S. Wiggins, and J. Hildebrand, "Humpback whale seasonal and spatial calling patterns in the temperate northeastern Pacific Ocean: 2008-2010," in *Proceedings of the 19th Biennial Conference on the Biology of Marine Mammals* (Tampa, FL, 2011), p. 53.
[23]P. J. Perkins, "Cornell laboratory of ornithology macaulay library: Humpback whale, *Megaptera novaeangliae*" (1973), http://macaulaylibrary.org/audio/110847 (Last viewed December 14, 2011).
[24]NOAA National Geophysical Data Center, "U.S. coastal relief model, Vol. 6," (2011), http://www.ngdc.noaa.gov/mgg/coastal/crm.html (Last viewed December 16, 2011).
[25]C. Amante and B. W. Eakins, "ETOPO1 1 Arc-Minute Global Relief Model: Procedures, Data Sources and Analysis," Technical Report, NOAA National Geophysical Data Center, Boulder, CO (2009), http://www.ngdc.noaa.gov/mgg/global/relief/ETOPO1/docs/ETOPO1.pdf (Last viewed March 2, 2013).
[26]T. Boyer, J. Antonov, O. Baranova, H. Garcia, D. Johnson, R. Locarnini, A. Mishonov, T. O'Brien, D. Seidov, I. Smolyar, M. Zweng, and S. Levitus, "World ocean database 2009," NOAA Atlas NESDIS **66**, pp. 1–116 (2009), ftp://ftp.nodc.noaa.gov/pub/WOD/DOC/wod09ntro.pdf (Last viewed March 2, 2013).
[27]Ocean Acoustics Group, Massachusetts Institute of Technology, "The Santa Barbara Channel Experiment" (1999), http://acoustics.mit.edu/sbcx (Last viewed May 12, 2012).
[28]E. Hamilton, "Sound velocity–density relations in sea-floor sediments and rocks," J. Acoust. Soc. Am. **63**, 366–377 (1978).
[29]E. Hamilton, "Sound velocity gradients in marine sediments," J. Acoust. Soc. Am. **65**, 909–922 (1979).
[30]C. Wentworth, "A scale of grade and class terms for clastic sediments," J. Geol. **30**, 377–392 (1922).
[31]W. Krumbein and L. Sloss, *Stratigraphy and Sedimentation* (W. H. Freeman and Co., New York, 1951), pp. 1–497.
[32]K. Marsaglia, K. Rimkus, and R. Behl, "Provenance of sand deposited in the Santa Barbara Basin at Site 893 during the last 155,000 years," in *Proceedings-Ocean Drilling Program Scientific Results* (National Science Foundation, Washington, DC, 1992), pp. 61–76.
[33]J. de Mesquita Onofre, "Analysis and modeling of the acoustic tomography signal transmission from Davidson Seamount to Sur Ridge: The forward problem," Master's thesis, Naval Postgraduate School (1999), http://www.nps.edu/Academics/GSEAS/oal/publications/jaonofre.pdf (Last viewed March 2, 2013).
[34]C. Gabriel, "The physical characteristics of bottom sediment near Sur Ridge, California," Master's thesis, Naval Postgraduate School (2001), http://www.dtic.mil/cgi-bin/GetTRDoc?Location=U2&doc=GetTRDoc.pdf &AD=ADA391676 (Last viewed March 2, 2013).
[35]J. Konter, H. Staudigel, J. Blichert-Toft, B. Hanan, M. Polvé, G. Davies, N. Shimizu, and P. Schiffman, "Geochemical stages at Jasper Seamount and the origin of intraplate volcanoes," Geochem., Geophys., Geosyst. **10**, Q02001 (2009).
[36]A. Nuttall, "Detection performance of power-law processors for random signals of unknown location, structure, extent, and strength," Technical Report, NUWC-NPT, Newport, RI (1994), http://www.dtic.mil/dtic/tr/fulltext/u2/a285868.pdf (Last viewed March 2, 2013).
[37]T. Marques, L. Munger, L. Thomas, S. Wiggins, and J. Hildebrand, "Estimating North Pacific right whale *Eubalaena japonica* density using passive acoustic cue counting," Endangered Species Res. **13**, 163–172 (2011).
[38]M. McDonald and C. Fox, "Passive acoustic methods applied to fin whale population density estimation," J. Acoust. Soc. Am. **105**, 2643–2651 (1999).
[39]W. Au, A. Pack, M. Lammers, L. Herman, M. Deakos, and K. Andrews, "Acoustic properties of humpback whale songs," J. Acoust. Soc. Am. **120**, 1103–1110 (2006).
[40]M. Collins, *User's Guide for RAM Versions 1.0 and 1.0p*, Naval Research Laboratory, Washington, DC (2002), http://www.siplab.fct.ualg.pt/models/ram/manual.pdf (Last viewed March 2, 2013).
[41]R. Urick, *Principles of Underwater Sound* (McGraw-Hill, New York, 1983), Vol. 3, pp. 19–22.
[42]T. Marques, L. Thomas, J. Ward, N. DiMarzio, and P. Tyack, "Estimating cetacean population density using fixed passive acoustic sensors: An example with Blainville's beaked whales," J. Acoust. Soc. Am. **125**, 1982–1994 (2009).
[43]A. Benda-Beckmann, F. Lam, D. Moretti, K. Fulkerson, M. Ainslie, S. van IJsselmuide, J. Theriault, and S. Beerens, "Detection of Blainville's beaked whales with towed arrays," Appl. Acoust. **71**, 1027–1035 (2010).